# Atmospheric-Pressure Plasma Deposited Epoxy-Rich Thin Films as Platforms for Biomolecule Immobilization—Application for Anti-Biofouling and Xenobiotic-Degrading Surfaces

Giuseppe Camporeale, Maryline Moreno-Couranjou,* Sébastien Bonot, Rodolphe Mauchauffé, Nicolas D. Boscher, Carine Bebrone, Cécile Van de Weerdt, Henry-Michel Cauchie, Pietro Favia, Patrick Choquet

In this work, an atmospheric-pressure dielectric barrier discharge process is exploited for the fast deposition of adherent epoxy-rich layers acting as a versatile platform for the efficient one-step biomolecule immobilization in mild aqueous conditions. Particular attention is given to the influence of the plasma process parameters on the chemical and morphological properties of the deposited layers and on their subsequent exploitation for chemical interfacial reactions. As a proof-of-concept, two enzymes with drastically different biological properties, namely dispersin B and a laccase, are immobilized onto functionalized metallic surfaces. The pH of the enzyme solution appears as a key parameter to control the amount of immobilized enzyme on the plasma functionalized surfaces, thus leading to bioactive surfaces with improved stability and activity.

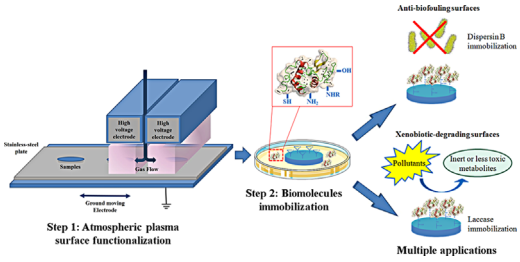


## 1. Introduction

Materials scientists are still inspired by nature for manufacturing materials presenting advanced surface properties based on the immobilization of enzymes onto solid surfaces. Enzymes are polyfunctional charged macromolecules composed of amino acid chains linked with peptide bonds and a more or less rigid three-dimensional structure.[1] Nowadays, immobilized enzymes have various practical applications in catalysis, analytics, therapeutics, and bio-separation, due to their several advantages. Among others, it can be reported an easy recovery of the product at the end of an enzymatically catalyzed reaction. Considering industrial applications, the possibility to reuse the immobilized enzymes leads to a significant cost saving. Finally, the surface immobilization might enhance the enzyme efficiency and stability compared to their free form in solution.[1,2] There are numerous approaches to irreversibly immobilize enzymes, including their inclusion/encapsulation into polymeric matrices, their crosslinking, or their covalent binding onto carrier materials.[3] This latter method is the most widely used and it is generally achieved

G. Camporeale, Prof. P. Favia
Dipartimento di Chimica, Università degli Studi di Bari "Aldo Moro", via Orabona 4, Bari 70126, Italy
Dr. M. Moreno-Couranjou, Dr. S. Bonot, R. Mauchauffé, Dr. N. D. Boscher, Dr. H.-M. Cauchie, Dr. P. Choquet
Luxembourg Institute of Science and Technology (LIST), 5 avenue des Hauts-Fourneaux, Esch/Alzette L-4362, Luxembourg
E-mail: moreno@lippmann.lu, maryline.moreno@list.lu
Dr. C. Bebrone, Dr. C. Van de Weerdt
Centre of Biomedical Integrative Genoproteomics (GIGA-R), University of Liège, B34 Sart-Tilman, Liège 4000, Belgium




DOI: 10.1002/ppap.201400206

through a nucleophilic substitution reaction between a modified/activated support and the enzyme amino-acid residues.

As an environmentally friendly technique, low-pressure plasma deposition processes have been successfully exploited for the deposition of adherent thin films functionalized with groups such as halogenide,[4] amino, carboxylic, hydroxyl, or epoxy[4–13] groups for the covalent bonding of a wide variety of peptides/proteins with biological activity retention.[14]

Considering industrial issues where each manufactured step must be connected to realize an efficient production line, the atmospheric-pressure (AP) plasma technology offers the possibility to be easily integrated into existing production systems, along with other advantages.[15] However, the exploitation of this technology remains scarcely reported in literature. Nisol et al.[16,17] have reported the elaboration of non-fouling coatings AP-plasma deposited by using a RF plasma torch in two different modes. The tetraglyme precursor was injected in the post-discharge zone either as a liquid (i.e., spray-AP plasma liquid deposition) or as a vapor (i.e., AP-plasma enhanced chemical vapor deposition). Recently, Da Ponte et al.[18] reported the successful deposition of non-fouling coatings using aerosol-assisted Atmospheric-Pressure Dielectric-Barrier-Discharges (AP-DBD) fed with helium. Concerning antibacterial surfaces, Chen et al.[19] used an atmospheric-pressure plasma jet fed with argon for polymerizing acrylic acid on silk fibers. The resulting carboxylic-functionalized surfaces were then exposed to an antibacterial peptide after an activation step. The potential of AP-DBD has been also demonstrated for the elaboration of such surfaces via the deposition of carboxylic and N-containing plasma interlayers.[20,21] However, despite promising results, these strategies present the drawback to rely on a multistep procedure, justifying thus the necessity to develop a novel one-step immobilization method.

Recently, Klages et al. reported the deposition of plasma polymer layer carrying a high density of epoxy groups by using a glycidyl methacrylate (GMA) monomer in an AP-DBD process.[22] The current work has a twofold objective: (i) a deeper understanding of the influence of AP-DBD process parameters on the chemistry and morphology of deposited epoxy-containing layers from GMA; (ii) the demonstration that these reactive interlayers can act as an efficient universal interlayer for one-step biomolecule immobilization. Hence, in the first part of the paper, it will be shown how adjustments of the plasma process parameters can allow to tune the morphology, the deposition rate, and the epoxy surface density of the deposited films. In a second part, as a proof of concept, epoxy rich layers will be exploited for the immobilization of two biomolecules. In particular, it will be reported and discussed how the pH of the solution used during the enzyme immobilization step can modify the coating biological performances.

## 2. Experimental Section

### 2.1. Materials

Plasma depositions were carried out on two kinds of substrates, namely: (i) mirror-polished stainless steel disks (304-8ND, AC&CS, 2 cm diameter, 1 mm thickness), used for Grazing Angle Fourier Transform-Infrared (FT-IR) measurements and biological tests and (ii) two face-polished silicon (111) wafers (Siltronix) for FT-IR analysis in transmission mode and SEM analysis. Conventionally polymerized poly(GMA) powder (Sigma-Aldrich, Mn ~20 000 g/mol) was also characterized for comparison.

Two enzymes with very different activities have been used in order to explore the possibilities of the epoxy-containing plasma functional layer as a platform for biomolecule immobilization. Enzymes immobilization on plasma treated samples was carried out in sterile polystyrene non-adhesive not-treated 12-well plates (Costar).

The first enzyme is dispersin B (DspB), a 42 kDa protein with anti-biofouling activity. It is active against both Gram negative and positive bacteria.[23] Its anti-biofouling activity was tested against the biofilm forming bacterial strain *Staphylococcus epidermidis* ATCC35984. DspB immobilization on plasma treated samples was carried out in sterile polystyrene 12-well plates (Thermo Scientific).

The medium used for the anti-biofouling tests are liquid Luria-Bertani (LB) medium, solid LB medium (LB agar), and liquid M63 medium. The composition of liquid LB medium for 1 L is 10 g of bactotryptone (BD Biosciences), 5 g of yeast extract (BD Biosciences), and 10 g of NaCl (VWR). Solid LB medium has a similar composition supplemented with 15 g of agar (VWR). M63 medium is composed of 100 mM $KH_2PO_4$ (VWR), 15 mM $(NH_4)_2SO_4$ (VWR), 16 mM $MgSO_4$ (VWR), 0.004 mM $FeSO_4$ (VWR), 0.5% casamino acids (VWR), 0.2% glucose (VWR), and KOH (VWR) for setting pH.

The second biomolecule chosen is a laccase (from *Pleurotus ostreatus*, Sigma-Aldrich), a non-specific hydrolase known to degrade many families of xenobiotics, including antibiotics.[24,25] Laccase degradation assays were carried out in sterile polystyrene non-adhesive not-treated 12-well plate (Costar). In the present study, the target xenobiotic is the sulfamethoxazole, an antibiotic used in human medicine and detected in residual waste water treatment plants.[26]

### 2.2. Film Deposition

The AP-DBD plasma source, depicted in Figure 1, consists of two high-voltage electrodes covered by alumina and a moving table as ground electrode with a gap distance of about 1 mm. In order to avoid border effect, the stainless steel substrates (1 mm thickness) are placed into a stainless steel plate with drilled hole of 1 mm deep. This latter is fixed on the table, which is moving at a 1 cm/s speed. The distance between the HV electrodes and the stainless steel plate of 1 mm is kept constant. A 15 standard liters per minute (slm) argon flow (99.999%, Air Liquide), used as carrier gas, was bubbled

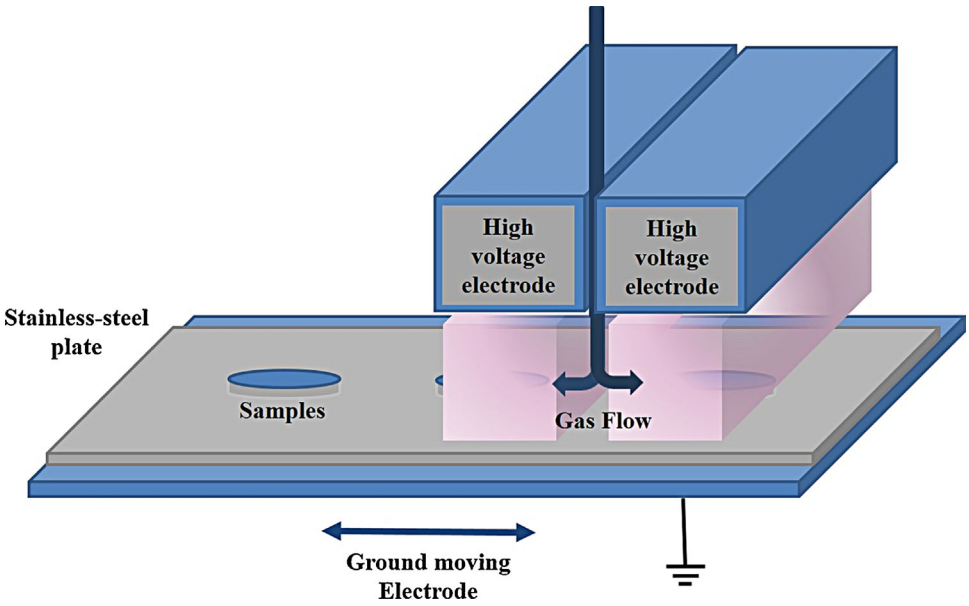


*Figure 1.* Schematic illustration of the AP-DBD source used for the layer deposition from GMA.

through the reservoir of GMA (≥97%, Sigma-Aldrich, Figure 2). Considering that GMA has a vapor pressure of 0.7 mbar at 20 °C[22] and assuming a complete saturation of the carrier gas stream with the GMA within the bubbler, the GMA flow rate was around 10.5 ml/min.

The plasma was generated using a "corona generator" 7010R (SOFTAL electronic GmbH) delivering a continuous or pulsed sinusoidal voltage signal, whose frequency was fixed at 10 kHz. Different depositions were carried out by adjusting the discharge mode, i.e., continuous (CW) or pulsed (PW) discharges, and by using a 50 W dissipated power ($P_{peak}$). The plasma-on time ($t_{on}$) was fixed at 10 ms, the plasma-off time ($t_{off}$) was varied from 10 to 80 ms. Hereafter, a suitable notation giving the $t_{on}$ and $t_{off}$ duration will be used. For example, 10:80 ms means that a 10 ms $t_{on}$ and a 80 ms $t_{off}$ were used. Average power densities ($P_{av}$) ranging from 0.2 to 2.8 W/cm$^2$ were tested. $P_{av}$ can be defined as follows:

$$P_{av} = P_{peak}[t_{on}/(t_{on} + t_{off})]/A$$

where $P_{peak}$ is the power of each plasma pulse and A is the electrode surface area.

Prior deposition, substrates were first cleaned by successive ultrasonic washings in butanone (5 min), acetone (1 min), and absolute ethanol (1 min) and further dried under a nitrogen flux. Then, substrates were activated through an Ar:$O_2$ (19/1 slm) plasma treatment in continuous mode at 1.6 W/cm$^2$ during 30 s. This Ar/$O_2$ plasma activation step aims to proceed to an ultimate cleaning of the surface of the substrate.[27,28] It is also performed in order to grow an oxide layer subsequently exploited for the better adhesion stability of the functional layer.

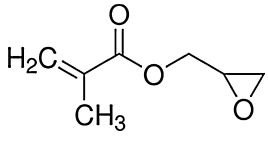


*Figure 2.* Chemical structure of glycidyl methacrylate (GMA).

### 2.3. Layer Characterization

Scanning electron microscopy (SEM) images were obtained with a Leica Stereoscan 430i (LEO) microscope after sputtering a 5 nm Pt thin film on the top of the plasma coating. The thickness of the plasma-polymerized GMA (ppGMA) deposited on silicon wafers was determined by examination of their cross-sections through SEM analysis. The plasma coated silicon wafers were broken along the cleavage plane by the help of a diamond tip cutter. It is a very conventional procedure to obtain cross-sections of coated silicon wafers for subsequent visualization. Before SEM investigation, however, the substrates were coated by a thin Pt layer in order to avoid charging effect. The film deposition rate was determined from the film thickness value and the total plasma deposition duration. The coating thickness measurements were carried out on at least three samples for each plasma deposition condition.

Atomic force microscopy (AFM) analysis was performed in ambient atmosphere using a PicoSPM LE instrument in intermittent-contact mode (Agilent Technologies). Topographic images were recorded at a 1 Hz scanning rate, 200–400 kHz resonance frequency, and 25–75 N m$^{-1}$ spring constants.

Fourier-transform infrared analysis was performed with a Bruker Hyperion 2000 spectrometer in transmission and in grazing angle modes (200 scans, 4000–500 cm$^{-1}$ range, 4 cm$^{-1}$ resolution). The epoxy content in the coatings was estimated by an integration of the 922–892 cm$^{-1}$ absorption band of normalized spectra according to the layer thickness and by using the OPUS software.

X-ray photoelectron spectroscopy (XPS) was carried out with a Kratos Axis Ultra DLD instrument (equipped with a monochromatic Al $K_\alpha$ X-ray source, $h\nu = 1486.6$ eV working at



DOI: 10.1002/ppap.201400206

50 W). The samples being insulating, a charge neutralizer producing low energy electrons of 3 eV was used. The energy calibration was done by fixing the main contribution (adventitious carbon and hydrocarbon) at 285.0 eV. The survey and narrow scans were acquired with 160 eV pass energy, 1 eV step size, 20 eV pass energy, and 0.1 eV step size, respectively. The XPS spectra were fitted with the CasaXPS software after subtraction of a Shirley type background. The XPS C1s signal was fitted into six different carbon chemical components,[29] namely: (i) C1: hydrocarbon ($C_xH_y$) at 285.0 eV; (ii) C2: secondary shifted carboxyl (C—CO—O) at 285.7 eV; (iii) C3: ether (C—O) at 286.7 eV; (iv) C4: epoxy at 287.0 eV; (iv) C5: ketone, aldehyde (C=O) or O—C—O at 287.8 eV; and (v) C6: ester (O—C=O) at 289.1 eV. For all components, the full width at half-maximum (FWHM) was kept between 1.1 and 1.3 eV. The peak contributions for the C—CO (C2) and O—C=O (C6) chemical groups were kept equal. The experimental uncertainty related to the XPS surface elemental composition is around 2 at %. For each deposition condition, at least two replicates were done and one point per sample (localized in the middle of the coating) was analyzed.

### 2.4. Expression and Purification of Recombinant Antibiofilm Dispersin B (DspB)

A strain of *Escherichia coli* is transformed with the introduction of a pET-28a/*DspB* plasmid (Life Technologies, UK). This plasmid is an expression vector for the DspB production allowing the obtention of DspB with an hexa-histidine tag at the *C*-terminal extremity of its sequence. The transformed bacteria was grown overnight at 37 °C with shaking in 50 ml LB medium supplemented with 50 μg/ml kanamycin. The bacterial suspension was diluted 100-fold in a total of 2 L of LB supplemented with kanamycin (50 μg/ml), and the expression of DspB was induced with isopropyl-β-D-thiogalactopyranoside (final concentration 0.5 mM). The induced culture was incubated for further 4 h (37 °C, shaking). DspB was purified by nickel affinity chromatography as previously described in the literature.[30] Fractions were analyzed by sodium dodecyl sulfate-polyacrylamide gel electrophoresis (SDS-PAGE) and by the ability to hydrolyze the chromogenic substrate 4-nitrophenyl-N-acetyl-β-D-galactosaminide (Sigma-Aldrich). Those fractions containing DspB were pooled and dialyzed against a 10 mM phosphate buffer at pH 5.9 with 100 mM NaCl overnight at 4 °C. Proteins were quantified using the BCA kit (Pierce).

### 2.5. Enzyme Immobilization on ppGMA Layers

#### 2.5.1. DspB immobilization

The ppGMA coated stainless-steel coupons were immersed in 1 mg/ml of DspB-containing 10 mM phosphate buffered solution with pH ranging from 7.0 to 8.5. The substrates were allowed to react for 1 h (ambient temperature, gentle agitation). Afterwards, the surfaces were rinsed with deionized water (4 times in 5 min, 250 rpm stirring) to remove unreacted proteins.

#### 2.5.2. Laccase immobilization

Laccase were immobilized on ppGMA coated stainless-steel 22 coupons through immersion in 1 ml of a 10 mM PBS containing 1 mg/ml laccase at pH 7.0 or 8.5 (1 h, room temperature, 150 rpm stirring).

In parallel, the enzymatic concentrations in solution were determined with the RC DC Protein Assay (Bio-Rad). The amount of immobilized laccase on the functionalized surfaces was estimated from the difference of laccase concentrations in solutionbefore and after the immobilization procedure.

### 2.6. *In Vitro* Antiadhesion Tests

A preculture of biofilm forming *S. epidermidis* ATCC35984 was grown overnight at 37 °C in a 3 ml Luria-Bertani (LB) media under 150 rpm agitation and used the next morning to seed a fresh culture in LB (50 ml). The bacterial concentration of test inoculum was adjusted to about $10^7$ cells/ml in M63 medium. Test inoculum (200 μl) was pipetted onto each substrate. After 24 h of incubation at 37 °C, the substrates were twice rinsed with 10 ml sterile deionized water to remove non-adherent bacteria and then, they were placed face downward in glass jars containing 500-fold-diluted LB (20 ml) and 4-mm glass beads. The jars were shaken and then, their contents were sonicated in a water bath (50–60 kHz) for 2 min. Adherent bacteria were counted by plating 10-fold dilution on LB agar. The plates were incubated at 37 °C overnight before the counting of the colony-forming units. The reported results in the publication are the averages of at least three replicates.

### 2.7. Degradation Assays

For the immobilized enzymes, an enzymatic activity was estimated by monitoring the sulfamethoxazole degradation over time. Enzymes were incubated in a 2 ml degradation medium composed of sterile MilliQ water, HEPES (12.5 mM) and sulfamethoxazole (100 μg/ml). Each 24 h, the degraded sulfamethoxazole concentration was estimated by absorbance measurement at 260 nm with a Synergy 2 Multi-Mode Plate Reader (Biotek). The medium was removed every 24 h. Wells were washed three times with filtered tap water and further filled with a fresh degradation medium.

For the free enzymes in solution, in the wells used for the first measurements ($t = 24$ h), 8 μg of enzymes were directly dissolved in a 2 ml degradation medium containing sulfamethoxazole at a 100 μg/ml concentration.

For all other wells, at time t0, enzymes were dissolved in a 300 μl medium containing 20 μg/ml of sulfamethoxazole. All wells were supplemented with the same media every 24 h. Also, 24 h prior to the enzymatic activity measurement, wells were amended with a 100 μg/ml antibiotic solution and supplemented to achieve a 2 ml final volume.

## 3. Results and Discussion

### 3.1. Influence of Process Deposition Conditions on Chemistry and Morphology of ppGMA Layers

The AP-DBDs fed with Ar and GMA and operating under continuous or pulsed discharges lead to the deposition of ppGMA films well adherent to the metallic substrates.

As shown in Figure 3, reporting the dependence of film deposition rate with $t_{off}$, one can notice that over the $t_{off}$ range investigated, pulsed discharges lead to higher growth film rates than the CW one, suggesting the occurrence of different deposition mechanisms during $t_{on}$ and $t_{off}$, which influence the chemistry and morphology of the deposited films.

SEM observations reported in Figure 4 reveal that, whatever the deposition conditions, pinhole-free coatings covering homogeneously the entire substrate surface are achieved. Interestingly, one can notice that the electrical discharge parameters are likely to affect both layer deposition rate and morphology. In particular, working in CW mode lead to rough nanostructured surfaces with an averaged roughness value (Ra) around 148 nm (Figure 2a and Table 1) and composed of an abundant amount of aggregates presenting an average size distribution of $94 \pm 11$ nm. This kind of topography is typical of coatings deposited through an atmospheric-pressure plasma-enhanced CVD process[31,32] and is related to higher plasma energy density favoring gas-phase reactions and surface etching. Pulsing the discharge leads to smoother layers with Ra value close to 24 nm at 10:80 ms conditions. Interestingly, compared to the layers deposited in CW, those deposited in 10:10 ms conditions have an intermediate roughness (Ra 43 vs. 148 nm), with a higher average feature size ($168 \pm 25$ nm). Finally, layers deposited at 10:80 ms are almost aggregate-free, which may indicate that the growth mechanism of these layers is largely controlled by predominant surface reaction.

FT-IR analysis (Figure 5) was carried out in order to study the chemistry of the deposited film. Particular attention was paid to the detection of the four epoxide characteristic peaks, namely the epoxide ring C—H stretching at 3063 $cm^{-1}$, the ring breathing mode at 1258 $cm^{-1}$, the asymmetric, and symmetric ring deformation bands at 910 and 852 $cm^{-1}$, respectively.[33] For the ppGMA layers deposited at 50 W in CW mode, all the above mentioned bands were barely detectable, suggesting that most epoxide rings were opened during the deposition. In contrast, epoxide bands were clearly noticeable for ppGMA deposited in pulsed mode. This result suggests the existence of two distinct layer growth mechanisms when depositions are carried out in continuous or pulsed mode. In particular, one can notice that increasing $t_{off}$ from 10 to 80 ms (i.e., decreasing the duty cycle) leads to increasing the epoxide bands intensity indicating a higher content of epoxide groups in the films. These results are in agreement with Klages et al.[22] demonstrating that pulsed AP-DBD allows the formation of coatings with high monomer structure retention due to chemical reactions occurring during the $t_{off}$ between intact monomer molecules and surface radical centers generated during the $t_{on}$ period.

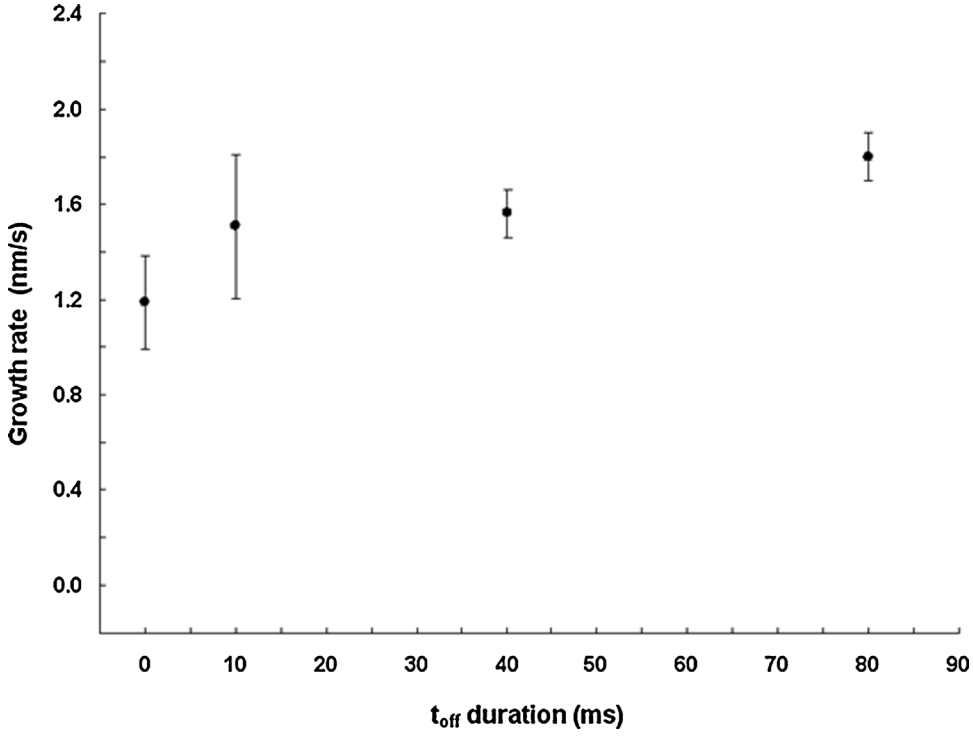


*Figure 3.* Evolution of the ppGMA film growth rate as a function of the plasma-off time ($t_{off}$), ranging from 0 (CW mode) to 80 ms ($t_{on}$ fixed at 10 ms; 50 W peak power).



DOI: 10.1002/ppap.201400206

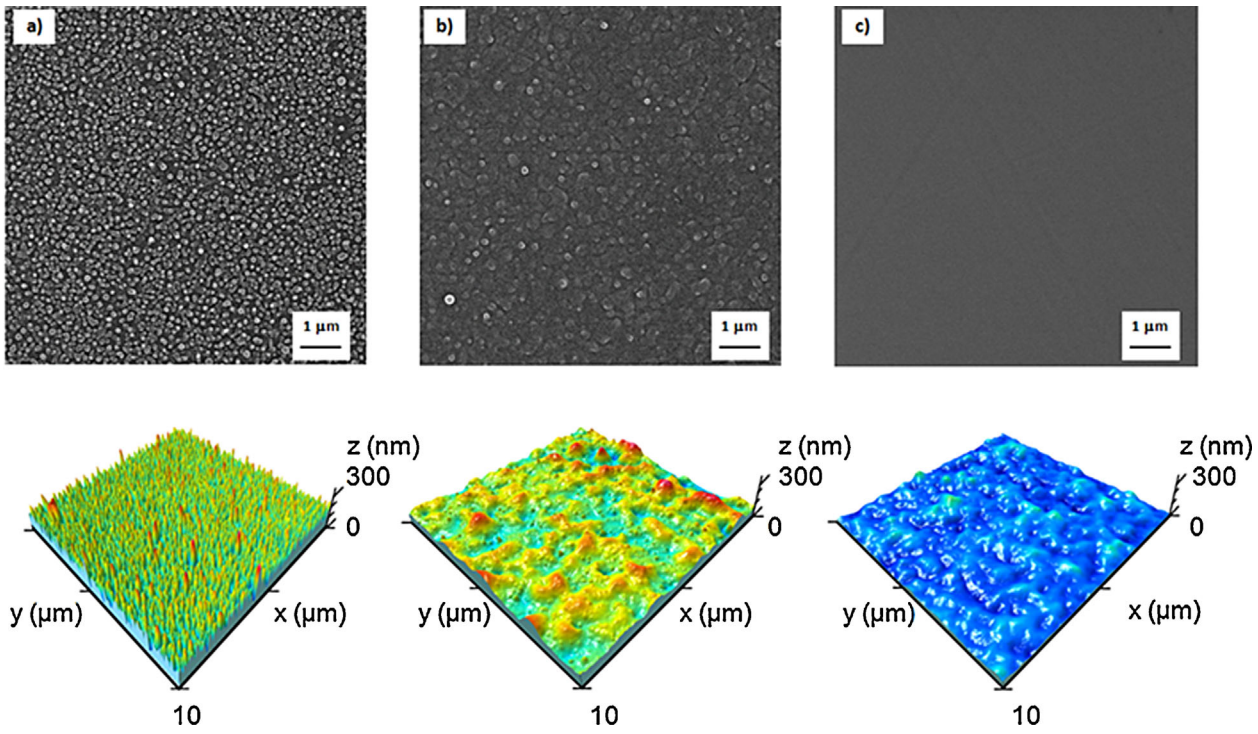


*Figure 4.* SEM (top) and AFM (bottom) pictures of ppGMA layers deposited at 50 W in CW mode (a) and 10:10 ms (b) and 10:80 ms PW modes (c).

To estimate the epoxide content in the ppGMA layers, the area of FT-IR asymmetric epoxide stretching band was calculated. Hence, as shown in Figure 6, it is concluded that working in pulsed mode allows to drastically increase the epoxy content in the deposited film up to a factor of 4.

In the aim of later exploiting chemical interfacial reactions between atmospheric-pressure plasma functionalized solid surfaces and free biomolecules, XPS analysis was carried out to get some insights concerning the ppGMA uppermost surface composition. In particular, this analysis allows to estimate the reactive epoxy surface density, a parameter which is reported to be strongly related to the biological performance of the functionalized surfaces.

Considering ppGMA deposited in CW mode, the XPS atomic percentages of the surfaces for the C:O elements were found to be equal to 77:23 (Table 2). Compared to the commercial poly(GMA) stoichiometry of 73:27, a lesser amount of oxygen was detected in the CW ppGMA layers, which might be correlated to the significant loss of the epoxy ring (i.e., monomer structure degradation), already highlighted in IR analysis (Figure 5). In contrast, it can be observed that PW deposited ppGMA layers and poly(GMA) present similar XPS compositions.

*Table 1.* Roughness values of ppGMA layers estimated by AFM measurements.

| Deposition conditions | Average roughness [Ra, nm] | Increment of surface area [%] |
|---|---|---|
| 50 W, CW | 148 ± 13 | 66.00 ± 1.00 |
| 50 W, 10:10 ms | 43 ± 8 | 0.20 ± 0.02 |
| 50 W, 10:80 ms | 24 ± 11 | 0.10 ± 0.04 |

The influence of the discharge mode (CW vs. PW) on the layer composition chemistry is particularly noticeable by overlapping their XPS C1s spectra (Figure 7). Indeed, one can clearly observe that a pulsed discharge allows a higher retention of the initial monomer ester group (C1s contribution at 289.1 eV) accompanied by the retention of epoxy groups (C1s contribution at 287.0 eV). In particular, from the XPS C1s curve-fitting data shown in Table 2, it appears that increasing the $t_{off}$ leads to an increase of the epoxy surface content with values ranging from 7 to 18 at. % for layers deposited at 10 and 80 ms $t_{off}$ duration, respectively. Interestingly, despite using mild process conditions, the maximal 27% epoxy content estimated for poly(GMA) is never reached in ppGMA layers. An explanation is that, despite a short $t_{on}$ duration, there is a non-negligible contribution of the film chemistry growth during this period associated with a high fragmentation of the monomer, and thus, a loss of the epoxy group. This theory is fully consistent with the results obtained in CW mode.

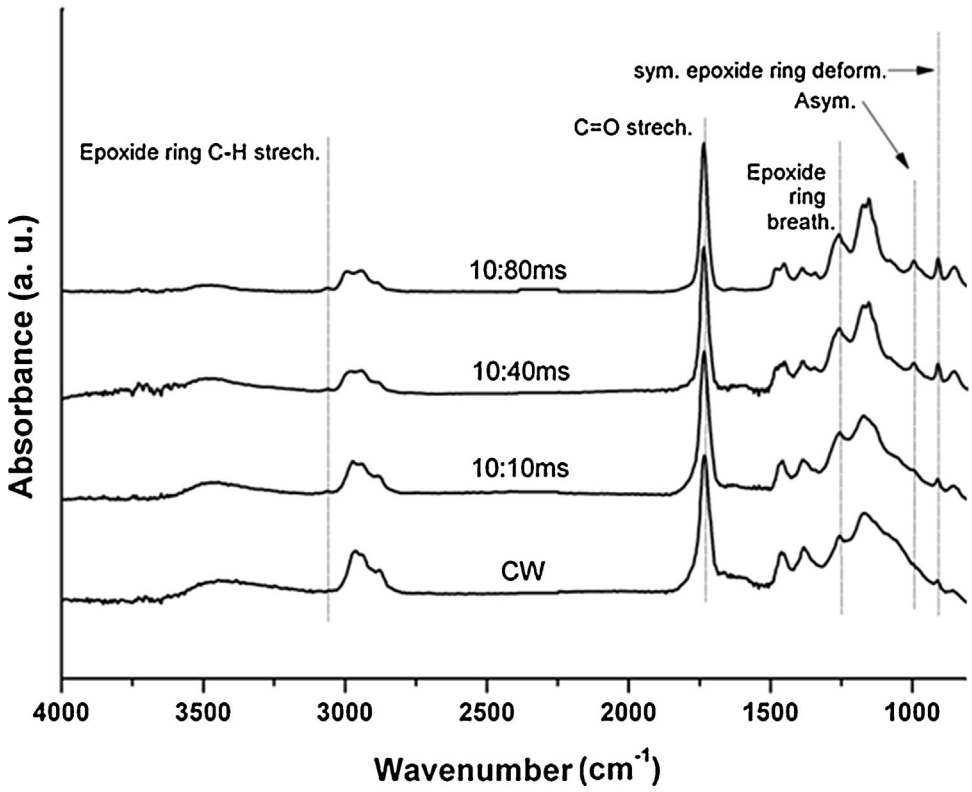


*Figure 5.* FT-IR spectra of ppGMA films deposited at 50 W with different duty cycles. All spectra were normalized to the maximum value of the C=O band (1735 $cm^{-1}$).

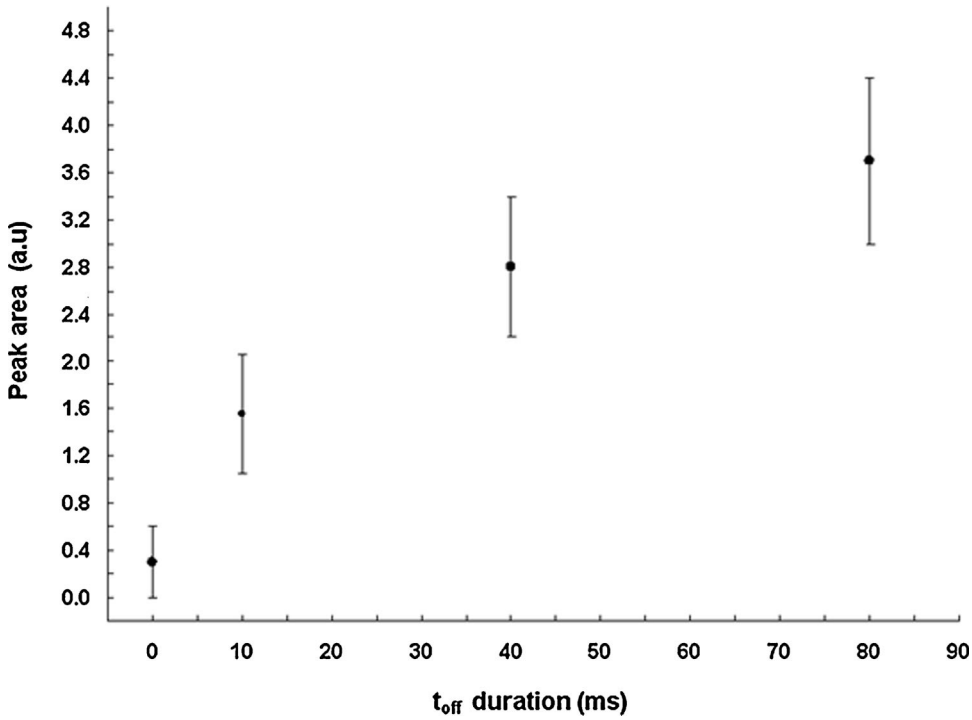


*Figure 6.* Area evolution of the FT-IR asymmetric epoxide ring deformation band as a function of the plasma-off time ($t_{off}$), ranging from 0 (CW mode) to 80 ms ($t_{on}$ fixed at 10 ms; 50 W peak power).



DOI: 10.1002/ppap.201400206

*Table 2.* XPS atomic percentages and C1s curve fitting data for ppGMA layers deposited in CW and PW modes. The results for a PW ppGMA layer after aging 50 d at air, and for a commercial poly(GMA) polymer are also reported.

| Samples | | | 50 W, CW | 50 W, 10:10 ms | 50 W, 10:80 ms | 50 W, 10:80 ms after 50 days at air | Poly(GMA) |
|---|---|---|---|---|---|---|---|
| **XPS surface composition [at. %]** | | | | | | | |
| | **C** | | 77 | 75 | 72 | 73 | 73 |
| | **O** | | 23 | 25 | 28 | 27 | 27 |
| **XPS C1s peak fitting, [%]** | | | | | | | |
| **Contribution** | **Binding energy [eV]** | **Functional group** | | | | | |
| C1 | 285.0 | C—C | 52 | 36 | 33 | 38 | 42 |
| C2 | 285.7 | C—CO—O | 8 | 11 | 13 | 12 | 11 |
| C3 | 286.7 | C—O | 25 | 25 | 22 | 25 | 8 |
| C4 | 287.0 | Epoxy | 0 | 7 | 18 | 9 | 27 |
| C5 | 287.8 | C═O/C—O—C | 5 | 10 | 2 | 4 | – |
| C6 | 289.1 | O—C═O | 8 | 11 | 13 | 12 | 11 |

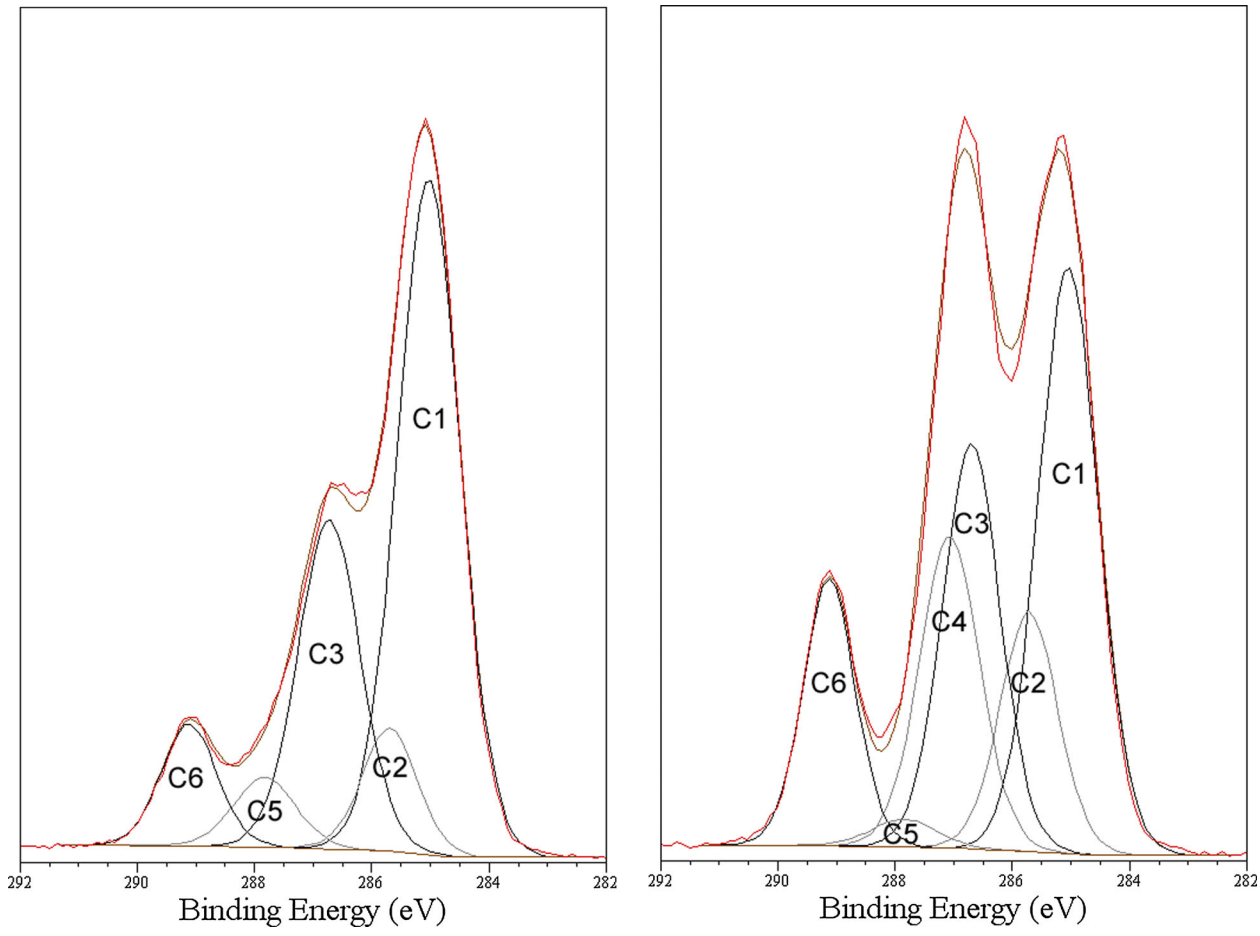


*Figure 7.* XPS C1s curve fittings for ppGMA layers deposited at 50 W, CW mode (left) and 50 W, 10:80 ms mode (right).

The aging of the richest epoxy ppGMA layer (i.e., 50 W, in 10:80 ms mode) was investigated through a 50-d storage period at ambient temperature and humidity. According to XPS analysis (Table 2), these storage conditions seem to have no significant influence on the layer composition that remains comparable to the poly(GMA)'s one, with C and O content equal to 73 and 27 at. %, respectively.

However, a careful C1s curve fitting allows highlighting a twofold decrease of the epoxy surface density down to 9% content, suggesting the relative chemical instability of epoxy groups.

In conclusion, it can be reported that, among the different plasma process conditions investigated, the pulsed atmospheric-pressure plasma polymerization of GMA carried out at 50 W in 10:80 ms allows for the fast deposition of adherent and smooth layers presenting the highest epoxy surface density, up to 18% (XPS data). Such freshly deposited ppGMA layers were selected in order to maximize the efficiency of biomolecule immobilization.[34]

### 3.2. DspB Immobilization and Anti-Biofouling Assessment

To ascertain the immobilization of DspB enzyme on the ppGMA layers, FT-IR analysis was carried out. From the data reported in Figure 8, one can notice that, independently of the pH of the DspB solution used during the immobilization step (i.e., pH = 7.0 or 8.5), ppGMA layers allow to efficiently immobilize the enzyme, as it is suggested by the appearance of new peaks related to peptide bonds, namely secondary amide N—H stretching, amide C═O stretching, and amide N—H bending bands located at 3281, 164, and 1539 $cm^{-1}$, respectively.[35] The peaks, characteristic of epoxide groups, at 1258, 910, and 852 $cm^{-1}$ are probably linked to their presence into the plasma film bulk, highlighting that the mild basic immobilization condition used does not lead to the epoxy loss through the ester group hydrolysis.

As reported in Table 3, independently of the pH of the DspB solution used during the immobilization steps, the DpsB-grafted coatings provide a comparable reduction of the number of viable adherent bacteria, up to 84%, after only 1 d of contact. This result highlights that this enzyme has maintained its anti-biofouling property even after its covalent immobilization on the ppGMA layers. The fact that the immobilized enzyme has kept its activity can suggest that its biological reaction sites have not been affected during the reaction with the ppGMA layer. The pH change during the enzyme grafting step has no effect on the final measured enzymatic activity. This

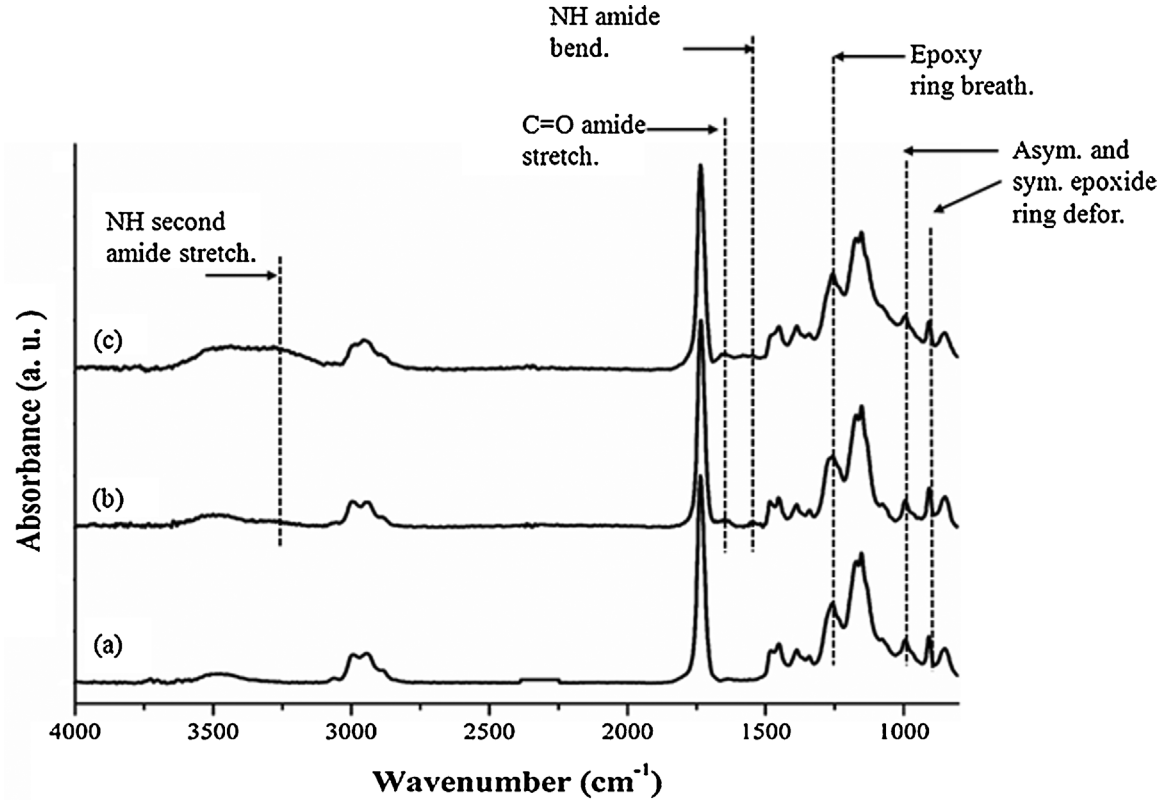


*Figure 8.* FT-IR spectra of freshly deposited ppGMA layers at 50 W in 10:80 ms (a), layer "a" after DspB immobilization at pH 7.0 (b), and pH 8.5 (c).



DOI: 10.1002/ppap.201400206

*Table 3.* Anti-biofouling activity against *S. epidermidis* biofilm forming of modified stainless-steel surfaces compared to uncoated ones.

| Samples | Reduction of adherent population [%] |
|---|---|
| Stainless steel | 0 |
| ppGMA layers | 0 |
| Dsp B immobilized at pH 7.0 | 79 ± 16 |
| Dsp B immobilized at pH 8.5 | 84 ± 11 |

suggests that the active immobilized enzyme amount is similar in both cases.

By reference with other works reported in the literature, the reason of this success can probably be associated with the presence of an hexahistidine tag (his-tag) added at the *C*-terminal extremity of the enzyme.[23] Kurzatkowska et al.[36] have already reported the exploitation of his-tag to ensure an enzyme immobilization in a proper orientation, or at least, to initiate an attachment which could then be supplemented by other interactions with the rest of the enzyme structure, and consequently, preventing or limiting the interaction and/or masking of the enzyme active site. Martin et al.[37] have also reported that his-tagged biomolecules can be covalently immobilized on supports through the nucleophilic reaction of the imidazole group (i.e., secondary amine) with the epoxy groups. In conclusion, if his-tag sequence has been initially introduced at the protein chain end to ensure its purification on a nickel affinity column during its production step, the present work highlights its usefulness for a covalent immobilization purpose.

### 3.3. Enzyme Immobilization for Xenobiotic Degradation

Irrespective of the pH (i.e., pH = 7.0 or 8.5) used during the enzyme immobilization step, pp-GMA layers allow the grafting of laccases, which are later active for the degradation of sulfamethoxazole. In Table 4, the average enzyme activity duration and the total quantity of degraded sulfamethoxazole for free and immobilized laccase are reported after different periods of time and Figure 9 shows their degradation kinetics.

All these results show clearly that the immobilization of the enzyme increases its efficiency and the duration of the enzymatic activity. By comparing the results between the test where the enzymes are in solution and the other one, where they are immobilized on a ppGMA surface at pH 7, it was observed that the total duration activity was multiplied by at least a factor of 4 (36 vs. 144 h for free and immobilized enzymes, respectively). Two hypotheses can support this interesting result. The first one can be attributed to the advantage of carrying out a strong enzyme immobilization through a multipoint anchorage. Indeed, this situation is known to confer a rigidity to the three-dimensional structure of the enzyme, thus, limiting breakdown and autolysis phenomena due to physico-chemical environmental factors.[38,39] The second one can be associated with the combined effect of pH and stirring when the enzymes are in solution. Indeed, these two parameters have been reported to promote free-form protein aggregation in solution[40] and to partly inactivate or neutralize enzymes.[3] In particular, the study of Shleev et al.[41] report that free-form laccase in phosphate buffer solution at pH 6.5, value closed of the experimental conditions, can be aggregated and/or inactivated.

In addition, the results show that during the enzyme immobilization, if the pH of the solution is lightly basic (pH = 8.5), the total amount of fixed enzyme is increased by a factor of 2. One hypothesis can be given to explain this result; it relies on the existence of different isoenzyme forms as it is known that pH can generate new rearrangement of the laccase periphery. Consequently, an improvement of the enzyme-plasma-treated surface interactions might be expected at pH 8.5.

Finally, it was also observed that bioactive layers generated at pH 8.5 present an increased xenobiotic degradation activity duration compared to the ones generated at pH 7.0 (240 vs. 144 h, respectively). More precisely, during the first 36 h of bioactivity, both surfaces presented a similar efficiency. However, after this time

*Table 4.* Summary of the averaged enzyme activity duration and the total quantity of degraded sulfamethoxazole for free and immobilized laccase. The quantity of immobilized enzymes on ppGMA layers is also reported.

| Assays | Averaged activity duration [h] | Quantity of immobilized enzyme [μg] | Quantity of degraded sulfamethoxazole for a 1 ml solution [μg] |
|---|---|---|---|
| Free enzyme in solution | 36 | – | 75 ± 5 |
| Laccase immobilized at pH 7.0 | 144 | 5.5 ± 4.0 | 174 ± 15 |
| Laccase immobilized at pH 8.5 | 240 | 12.0 ± 1.0 | 275 ± 14 |

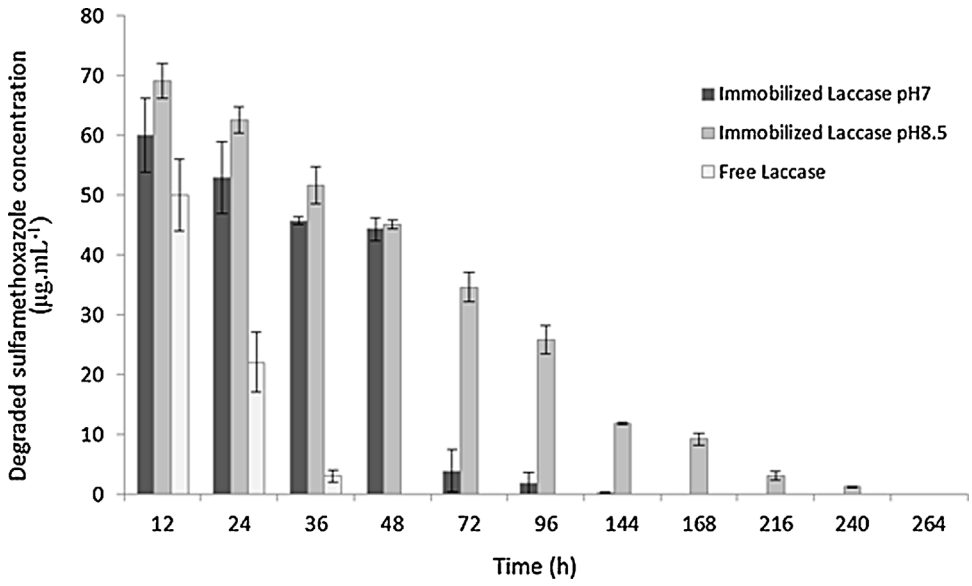


*Figure 9.* Activity of free and immobilized laccase.

lapse, the laccase activity set at pH 7.0 sharply decreased while the enzymatic activity of active layer generated at pH 8.5 slowly decreases until to reach 0 after 240 h. One explanation might come from the increased amount of fixed enzymes. Indeed, the density of immobilized proteins might have an influence on the three-dimensional structure of the protein due to the existence of numerous and deleterious protein-surface interactions. As reported by Tiller et al.,[42] when the surface of a substrate is covered with a high density of immobilized proteins, there are few possible interactions between the protein and the substrate, thus ensuring probably the integrity of the three-dimensional protein structure and the preservation of its enzymatic activity. In conclusion, these results highlight the importance of a well-adapted pH solution selection for the enzyme immobilization step.

## 4. Conclusion

A novel atmospheric-pressure method has been developed to efficiently immobilize enzymes onto solid surfaces, based on the AP-DBD deposition of an epoxy-rich layer and its subsequent interfacial one-step reaction with biomolecules in mild aqueous conditions. The method has highlighted that it is possible: (i) to modify the coating morphology by the use of continuous or pulsed discharges; (ii) to tune the epoxy surface density by adjusting the $t_{on}/t_{off}$ ratio; and (iii) to optimize the amount of grafted enzymes by selecting an appropriate pH during the immobilization step. Here, bioactive surfaces with anti-biofouling and xenobiotic degrading properties have been successfully elaborated. In particular, the immobilized laccase on ppGMA layers present an extended duration activity and efficiency around four and seven times higher than for the free enzyme in solution, respectively. Importantly, these results tend to show the versatility of the method as these epoxy-rich layers might offer the possibility to immobilize different functional biomolecules paving the way to the elaboration of novel advanced bioactive materials.

Acknowledgements: This research was carried out in the framework of the European M-ERA.NET BioADBD project funded by the Luxembourgish agency "Fonds National de la Recherche" (FNR-INER/MAT/11/01) and the DG06-Région Wallone agency (n° convention 111278). Dr. S. Bonot and Dr. H. M. Cauchie worked on the present topic within the frame of the ENZO project. The authors would like to thank Dr. P. Lassaux and J. Delbecq from GIGA-R for the skilful biological tests. Dr. J. Guillot, J. Didierjean, and P. Grysan from LIST are hereby gratefully acknowledged for their skilful characterizations and valuable discussions.

Received: October 24, 2014; Revised: February 27, 2015; Accepted: March 30, 2015; DOI: 10.1002/ppap.201400206

Keywords: atmospheric-pressure dielectric barrier discharges; bioactive surfaces; immobilization of biomolecules; plasma polymerization; plasma-enhanced chemical vapor deposition (PECVD)

[1] W. Tischer, F. Wedekind, *Top. Curr. Chem.* **1999**, *200*, 96.
[2] S. Aggarwal, S. Sahni, *Int. Conf. Environ. Biomed. Biotechnol.* **2012**, *41*, 18.

[3] B. M. Brena, F. Batista-Viera, *"Methods in Biotechnology: Immobilization of Enzymes and Cells"*, 2nd edition, J. M. Guisan, Ed., Humana Press Inc, Totowa, NJ **2006**.
[4] J. D. McGettrick, T. Crackford, W. C. E. Shofield, J. P. S. Badyal, *Appl. Surf. Sci.* **2009**, *256S*, S30.
[5] C. Vreuls, G. Zocchi, B. Thierry, G. Garitte, S. S. Griesser, C. Archambeau, C. Van de Weerdt, J. Martial, H. Griesser, *J. Mater. Chem.* **2010**, *20*, 8092.
[6] B. Thierry, M. Jasieniak, L. C. P. M. de Smet, K. Vasilev, H. J. Griesser, *Langmuir* **2008**, *24*, 10187.
[7] L. Chu, W. Knoll, R. Förch, *Biosens. Bioelectron.* **2008**, *24*, 118.
[8] L. De Bartolo, S. Morelli, A. Piscioneri, L. C. Lopez, P. Favia, R. d'Agostino, E. Drioli, *Biomol. Eng.* **2007**, *24*, 23.
[9] L. C. Lopez, M. G. Buonomenna, E. Fontananova, G. Iacoviello, E. Drioli, R. d'Agostino, P. Favia, *Adv. Funct. Mater.* **2006**, *16*, 1417.
[10] E. Sardella, L. Detomaso, R. Gristina, G. S. Senesi, H. Agheli, D. S. Sutherland, R. d'Agostino, P. Favia, *Plasma Process. Polym.* **2008**, *5*, 540.
[11] L. De Bartolo, S. Morelli, L. C. Lopez, L. Giorno, C. Campana, S. Salerno, M. Rende, P. Favia, L. Detomaso, R. Gristina, R. d'Agostino, E. Drioli, *Biomaterials* **2005**, *26*, 4432.
[12] M. Kastellorizios, G. P. K. Michanetzis, B. R. Pistillo, S. Mourtas, P. Klepetsanis, P. Favia, E. Sardella, R. d'Agostino, Y. F. Missirlis, S. G. Antimisiaris, *Int. J. Pharm.* **2012**, *432*, 91.
[13] S. Pavlica, S. Schmitmeier, P. Gloeckner, A. Piscioneri, F. Peinemann, K. Krohn, M. Siegmund-Schulz, S. Laera, P. Favia, L. D. Bartolo, A. Bader, *J. Tissue Eng. Regen. Med.* **2012**, *6*, 486.
[14] B. R. Coad, M. Jasieniak, S. S. Griesser, H. J. Griesser, *Surf. Coat. Technol.* **2013**, *233*, 169.
[15] G. Da Ponte, E. Sardella, F. Fanelli, R. d'Agostino, P. Favia, *Eur. Phys. J. Appl. Phys.* **2011**, *56*, 24023.
[16] B. Nisol, C. Poleunis, P. Bertrand, F. Reniers, *Plasma Process. Polym.* **2010**, *7*, 715.
[17] B. Nisol, G. Oldenhove, N. Preyat, D. Monteyne, M. Moser, D. Perez-Morga, F. Reniers, *Surf. Coat. Technol.* **2014**, *252*, 126.
[18] G. Da Ponte, E. Sardella, F. Fanelli, R. d'Agostino, R. Gristina, P. Favia, *Plasma Process. Polym.* **2012**, *9*, 1176.
[19] G. Chen, M. Zhou, Z. Zhang, G. Lv, S. Massey, W. Smith, M. Tatoulian, *Plasma Process. Polym.* **2011**, *8*, 701.
[20] R. Mauchauffé, M. Moreno-Couranjou, N. D. Boscher, C. Van De Weerdt, A-S. Duwez, P. Choquet, *J. Mater. Chem. B* **2014**, *2*, 5168.
[21] D. Duday, C. Vreuls, M. Moreno, G. Frache, N. D. Boscher, G. Zocchi, C. Archambeau, C. Van De Weerdt, J. Martial, P. Choquet, *Surf. Coat. Technol.* **2013**, *218*, 152.
[22] C.-P. Klages, K. Höpfner, N. Kläke, R. Thyen, *Plasmas Polym.* **2000**, *5*, 79.
[23] J. B. Kaplan, C. Ragunath, N. Ramasubbu, D. H. Fine, *J. Bacteriol.* **2003**, *185*, 4693.
[24] S. Rodríguez Couto, J. L. Toca Herrera, *Biotechnol. Adv.* **2006**, *24*, 500.
[25] C. E. Rodríguez-Rodríguez, M. A. García-Galán, P. Blánquez, M. S. Díaz-Cruz, D. Barceló, G. Caminal, T. Vicent, *J. Hazard Mater.* **2012**, *213–214*, 347.
[26] A. Göbel, A. Thomsen, C. S. McArdell, A. Joss, W. Giger, *Environ. Sci. Technol.* **2005**, *39*, 3981.
[27] G. Baravian, D. Chaleix, P. Choquet, P. L. Nauche, V. Puech, M. Rozoy, *Surf. Coat. Technol.* **1999**, *115*, 66.
[28] J. M. Thiébaut, T. Belmonte, D. Chaleix, P. Choquet, G. Baravian, V. Puech, H. Michel, *Surf. Coat. Technol.* **2003**, *169–170*, 186.
[29] G. Beamson, D. Briggs, *"High Resolution XPS of Organic Polymers. The Scienta ESCA 300 Database"*, Wiley-VCH, New York **1992**.
[30] E. Faure, C. Falentin-Daudré, T. S. Lanero, C. Vreuls, G. Zocchi, C. Van De Weerdt, J. Martial, C. Jérôme, A.-S. Duwez, C. Detrembleur, *Adv. Funct. Mater.* **2012**, *22*, 5271.
[31] A. Manakhov, M. Moreno-Couranjou, N. D. Boscher, V. Rogé, P. Choquet, J.-J. Pireaux, *Plasma Process. Polym.* **2012**, *9*, 435.
[32] H. Hody, P. Choquet, M. Moreno-Couranjou, R. Maurau, J.-J. Pireaux, *Plasma Process. Polym.* **2010**, *7*, 403.
[33] C. Tarducci, E. J. Kinmond, J. P. S. Badyal, S. A. Brewer, C. Willis, *Chem. Mater.* **2000**, *12*, 1884.
[34] L. Cao, *"Carrier-Bound Immobilized Enzymes"*, Wiley, Weinheim, Germany **2005**.
[35] B. Smith, *Infrared Spectral Interpretation. A Systematic Approach"*, 2nd edition, CRC Press LLC, Bocar Raton, FL **1999**.
[36] K. Kurzątkowska, M. Mielecki, K. Grzelak, P. Verwilst, W. Dehaen, J. Radecki, H. Radecka, *Talanta* **2014**, *130*, 336.
[37] M. T. Martin, F. J. Plou, M. Alcalde, A. Ballesteros, *J. Mol. Catal. B: Enzym.* **2003**, *21*, 299.
[38] H.-C. Mahler, W. Friess, U. Grauschopf, S. Kiese, *J. Pharm. Sci.* **2009**, *98*, 2909.
[39] C. Garcia-Galan, A. Berenguer-Murcia, R. Fernandez-Lafuente, R.-C. Rodrigues, *Adv. Synth. Catal.* **2011**, *353*, 2885.
[40] C. Mateo, V. Grazù, B. C. Pessela, T. Montes, J. M. Palomo, R. torres, F. López-Gallego, R. Fernández-Lafuente, J. M. Guisán, *Biochem. Soc. Trans.* **2007**, *35*, 1593.
[41] S. Shleev, C. T. Reimann, V. Serezhenkov, D. Burbaev, A. I. Yaropolov, L. Gorton, T. Ruzgas, *Biochimie* **2006**, *88*, 1275.
[42] J. C. Tiller, R. Rieseler, P. Berlin, D. Klemm, *Biomacromolecules* **2002**, *3*, 1021.